Enhanced electron-phonon coupling of Ti-doped superconducting Nb_3Sn films investigated at microwave frequencies

M. Perpeet
Bergische Universität Wuppertal, Fachbereich C, 42097 Wuppertal, Germany

M. A. Hein
Technische Universität Ilmenau, Electrical Engineering and Information Technology, P.O. Box 100565, 98684 Ilmenau, Germany
(Received 2 December 2004; revised manuscript received 17 June 2005; published 7 September 2005)

The intermetallic superconductor Nb_3Sn is an interesting reference system, due to its high transition temperature and strong coupling, to compare with superconductors like MgB_2 or the cuprates. We have prepared high-quality stoichiometric Nb_3Sn films on sapphire by tin vapor diffusion. This technique enabled controlled doping of Nb_3Sn films with Ti, which substitutes for Nb along the quasi-one-dimensional chain sites. The microwave response of the films was studied at 87 GHz using a cavity-endplate technique. The temperature-dependent surface resistance of undoped films was in perfect agreement with the predictions of strong-coupling theory. However, the behavior of the penetration depth contradicted them, showing an unexpected weakly curved temperature dependence. Ti doping affected this behavior. Increasing the Ti concentration introduced a monotonically increasing curvature of $\Delta\lambda(T)$. Furthermore, key superconducting properties like the reduced energy gap Δ/kT_c and the quasiparticle conductivity underwent nonmonotonic changes for increasing Ti concentration. Our observations are analyzed in terms of impurity scattering and changes of the electron-phonon coupling strength, most likely resulting from an altered quasiparticle density of states at the Fermi level.

DOI: 10.1103/PhysRevB.72.094502 PACS number(s): 74.25.Nf, 74.62.Dh, 74.70.Ad, 74.78.Db

I. INTRODUCTION

Despite the advent of, e.g., the cuprate superconductors[1] and, more recently, the diboride MgB_2,[2] studies of the classical A15 superconductors like Nb_3Sn remain interesting. From a fundamental point of view, Nb_3Sn is the only established strongly coupled *s*-wave high-temperature superconductor [electron-phonon coupling constant $\lambda_{ep} \sim 1.5$ (Ref. 3)]. The high values for the transition temperature and the superconducting energy gap were associated with the face-centered-cubic Sn lattice, superimposed by three pairs of orthogonal Nb chains, leading to distinctive peaks in the quasiparticle density of states (DOS) $N_N(E)$.[4] As confirmed by band-structure calculations and spectroscopic measurements for Nb_3Sn, these singularities occur at energies close to the Fermi energy E_F, thus giving rise to its outstanding superconducting properties.[5,6] Similar mechanisms have been proposed for the layered cuprate superconductors.[7]

In Ref. 8, we reported the successful deposition of phase-pure Nb_3Sn films on sapphire using a two-step process. This enabled the synthesis of samples of reproducible high quality, superior to films prepared by other techniques like sputtering or co-evaporation.[9,10] Remarkably, all investigated samples revealed an unexpected temperature dependence of the penetration depth. A significantly weaker curvature of $\lambda(T)$ than expected from strong-coupling theory was observed. At temperatures $T < 0.5T_c$, the temperature dependence followed a linear rather than an exponential dependence.

The temperature dependence of the penetration depth reflects the pairing mechanism of the charge carriers forming the superfluid condensate, and thus the quasiparticle DOS. It can provide information on, e.g., scattering, electron-phonon coupling strength, or the symmetry of the order parameter. A linear or quadratic temperature dependence, for instance, can hint at a *d*-wave symmetry of the order parameter, as is the case for the cuprates.[11] In terms of MgB_2, the uncommon $\lambda(T)$ is discussed in the frame of a two-gap model,[12] while the exponential temperature dependence identifies it as an *s*-wave superconductor.

To gain deeper insight into the electronic material properties and their interaction with the crystal lattice, electronic doping is a suitable tool. From experiments with Nb_3Sn wires, Ti is known to be a well-suited dopant, as it replaces the Nb atoms within the chains.[13] This implies a conspicuous effect on the superconducting properties. Doping studies of Nb_3Sn have been performed predominantly on bulk material and wires, due to the often poor and hardly reproducible quality of films. We report here systematic Ti-doping studies of high-quality Nb_3Sn films on sapphire.

Microwave measurements present a sensitive technique to analyze the dynamics of normal and superconducting charge carriers, and hence the quasiparticle scattering and pair condensation.[14] The experimental data permit the deduction of values for the energy gap Δ_0, London penetration depth λ_L, coherence length ξ_0, and electron mean free path l. These parameters, in combination with microscopic theories, give insight into the electron-phonon coupling strength and quasiparticle DOS in the normal and superconducting states.[15]

II. EXPERIMENTAL TECHNIQUES

A. Deposition of Nb_3Sn films

The Nb_3Sn films were prepared by a two-step process.[8,16] First, a Nb-precursor film was sputtered onto a sapphire sub-

TABLE I. Characteristic parameters deduced from *RF* measurements and confirmed by shielding and tunneling investigations. For comparison, typical values taken from the literature are added. λ_0 describes the upper limit of λ_L, as described in the text.

	T_c (K)	Δ/kT_c	λ_L (nm)	l (nm)	ξ_0 (nm)
RF measurement	18.0±0.10	2.01±0.10	91.1±2.1	12.1±1.2	6.8±0.5
Inductive/tunneling	18.0±0.05	2.00±0.13	90.9±2.2		6.7±0.3
Co-evaporation[a]	16.0–17.9	1.2–2.1	90–100	2–10	5.7–7.7
Sputtering[b]	16.5–18.0	1.3–1.9	$\lambda_0 \cong 600$		

[a]Reference 10.
[b]Reference 9.

strate (10 mm × 10 mm), which was subsequently converted to Nb_3Sn by Sn-vapor diffusion. This process yielded stoichiometric phase-pure films with a granular structure. The columnar grains exhibit average diameters d_G up to 1.4 μm.[17] Table I summarizes typical superconducting parameters deduced from microwave data[18] and supplemented by measurements of inductive shielding and electronic tunneling properties.[16] The data confirm the high quality of the samples, compared with typical values from the literature.[9,10] Additionally, the consistency among the different measurements is convincing. The high reproducibility is documented by the small parameter scattering, stated as the errors in Table I. These values imply that the electronic response of the samples falls into the local limit ($\xi_0 \ll \lambda_L$), while, considering the electronic mean free path, the response indicates an intermediate state, i.e., between the clean and dirty limits ($l \cong \xi_0$).[19]

The high quality of our Nb_3Sn films is a direct consequence of the Sn-vapor diffusion, which is a well-established technique applied to metallic surfaces, e.g., for Nb_3Sn-coated Nb cavities for superconducting particle accelerators.[20] The technique has proven to yield Nb_3Sn layers of excellent structural properties in terms of stoichiometry, Sn distribution, and phase purity, with extremely good superconducting properties (like large energy gap and low residual surface resistance). Our earlier studies showed that Sn-vapor diffusion can be favorably applied also to Nb films on dielectric substrates like single-crystal sapphire, yielding a comparably high material quality.[8,16–18,21]

B. Ti doping

Ti-doped films were obtained by diffusing Sn into the Nb-precursor films that had layers of Ti implemented. A similar process was reported in Ref. 13 for Ti-doped wires.

The Nb-Ti-Nb sandwiches were prepared by planar dc-magnetron sputtering in an argon atmosphere (partial pressure of 0.9 Pa), after the sputtering chamber had been evacuated to a residual pressure of 8×10^{-5} Pa. The sputtering was performed at room temperature, with a plasma power of 80 W, yielding typical deposition rates of 94 nm/min. All samples were prepared with a total Nb-layer thickness of 1.88 μm, reflecting a fixed total-deposition time of 20 minutes. The thickness (20 to 240 nm) and the number n of the Ti layers (n=1 to 4) were adjusted according to the desired total amount of Ti. To alter the diffusion of the Ti atoms into the Nb precursor, an additional tempering step was introduced for some samples. These samples were kept at a temperature of 1360 °C under ultrahigh vacuum (8×10^{-5} Pa) for 28 hours. Like the undoped films, the as-grown and the annealed Nb-Ti sandwich structures were then subjected to the Sn-diffusion process at a temperature of 1100 °C for 6 h. Due to the conversion, the thickness d_F of the resulting Nb_3Sn:Ti films increased by a factor of about 4/3 compared to the Nb precursors. The thickness ranged between 2.53 and 2.83 μm, which was in accordance with the expectations, considering the similar atomic masses and densities of Nb (8.59×10^3 kg/m^3) and Nb_3Sn (8.92×10^3 kg/m^3). In total, 16 Ti-doped samples of different concentration were prepared and characterized.

The total amount of Ti was chosen to cover a range of nominal concentrations of $c_{Ti} \approx 0.5$ to 9 at. %, assuming homogeneous Ti diffusion. The normal-state resistivity $\rho_N(T_c)$, deduced from surface-resistance data in the normal skin-effect limit, scaled linearly with c_{Ti}, as illustrated in Fig. 1(a). This behavior is consistent with the assumption that the Ti atoms cause additional scattering centers. While the linear dependence agrees qualitatively with the results of Ref. 13 [Fig. 1(b)], the nominal sensitivity $\partial\rho/\partial c_{Ti} \cong 3.8$ $\mu\Omega$ cm/at. % of our films is weaker by a factor of about 4 than in Ref. 13. Interestingly, the slopes extracted for the multilayer structures (2.2 $\mu\Omega$ cm/at. %) and the an-

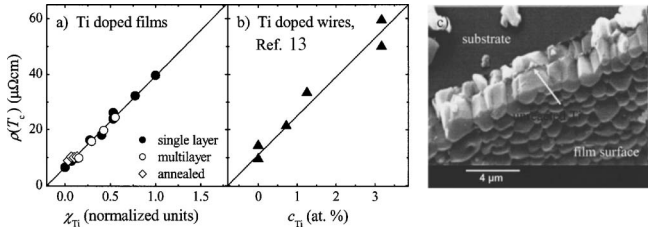

FIG. 1. (a) Linear variation of the normal-state resistivity $\rho_N(T_c)$ and the effective Ti concentration χ_{Ti}, measured for single-layer Nb_3Sn:Ti films (filled circles), multilayer films (open circles), and subsequently annealed samples (diamonds). The Ti concentration is given in normalized units, as explained in the text. (b) Displays data for Ti-doped Nb_3Sn wires (Ref. 13) for comparison. A SEM picture of the cross section of the highest-doped sample (χ_{Ti}=1) is shown in (c). Element analysis revealed residues of unreacted Ti, as indicated by the arrow.

nealed samples (0.5 $\mu\Omega$ cm/at. %) were even lower.

These observations indicate an inhomogeneous distribution of the Ti in the Nb_3Sn:Ti films, given that the microwave measurements sense the effective film composition only within about one skin-depth beneath the surface. At 87 GHz, the values of the skin depth range from about 230 to 530 nm, covering less than 20% of the entire film thickness. A preparation-dependent concentration gradient could indeed be confirmed by spectral analysis of the film composition. From scanning electron microscopy (SEM) of the cross section of cracked samples, structural inhomogeneities were observed, which could be associated with residues of the original Ti layers. For the two highest doping concentrations, even traces of unreacted Ti were found, as illustrated in Fig. 1(c). These observations support the assumption that the Ti diffusion remained incomplete after finishing the conversion process.

The resistivity data, therefore, cannot be used as an absolute, but merely a relative, measure of the Ti concentration. Based on the linear variation of $\rho_N(T_c)$ with the Ti concentration, an effective doping χ_{Ti} can be defined, by scaling the dependences for the various sets of films onto a single linear relation. The resulting values were then normalized to the highest investigated concentration level, as eventually adopted for Fig. 1(a).

C. Microwave measurements

The microwave measurements were performed at 87 GHz using a cylindrical Cu-cavity resonator with the sample replacing one endplate.[22] The temperature-dependent quality factor and frequency shift were measured for temperatures between 4.2 K and room temperature. The raw data were evaluated by the fully computer-controlled system in terms of the complex-valued surface impedance $Z_S(T)$, i.e., the surface resistance $R_S(T)$ and the change of the penetration depth $\Delta\lambda(T)$. All measured data were corrected for the finite film thickness and the sensitivity limit of the measurement system (0.5 mΩ), as described in Ref. 22.

III. THEORETICAL BACKGROUND

The linear interaction of a superconductor with an electromagnetic field, whose frequency is sufficiently below the gap frequency ($\omega \ll \Delta/\hbar$), is described, in momentum space, by an expression relating the quantum-mechanical current density $J(q,\omega,T)$ to the magnetic vector potential $a(q,\omega)$ (q denotes the wave vector).[23]

$$J(q,\omega,T) = \frac{1}{\mu_0} K(q,\omega,T) a(q,\omega). \tag{1}$$

The complex-valued response function $K(q,\omega,T)$ reflects the material properties and represents a generalized form of the complex conductivity

$$\frac{-iK}{\omega\mu_0} = \sigma = \sigma_1 - i\sigma_2. \tag{2}$$

The real and imaginary parts of the conductivity correlate with the temperature-dependent fraction of normal charge carriers $n_N(T) \propto \sigma_1$ and superconducting charge carriers $n_S(T) \propto \sigma_2$. In the clean local limit, the two fractions are related by the simple two-fluid model expression $n_N(T) = 1 - n_S(T)$, with $n_S(T) \propto 1/\omega\mu_0\lambda_L^2(T)$.

Microscopically, the superfluid density can be related to the quasiparticle DOS by (Ref. 24)

$$\frac{\lambda_0^2}{\lambda^2(T)} = 1 - 2\int_0^\infty \left(-\frac{\partial f(\varepsilon,T)}{\partial\varepsilon}\right)\frac{N_S(\varepsilon,T)}{N(0)}d\varepsilon, \tag{3}$$

with the Fermi distribution function $f(\varepsilon)$ and the relative energy scale $\varepsilon = E - E_F$. The condensation of quasiparticles into Cooper pairs, in BCS theory, leads to the typical s-wave DOS $N_S(\varepsilon) = N_N(0) \times [1 - (\Delta_0/\varepsilon)^2]^{-1/2}$, causing the well-known activated temperature dependence $\exp[(-\Delta/k_B T_c) \times T_c/T]$. Electronic interactions like, e.g., scattering, strong coupling, or pair breaking, must be considered in addition, causing a rounding and broadening of the square-root singularity, or creating quasiparticle states within the gap. Similar behavior arises if the order parameter deviates from the s-wave symmetry. In turn, all these effects have an impact on the conductivity $\sigma(T)$, possibly even turning the exponential temperature dependence into a power-law behavior.[25]

The quantum-mechanical coherence among all quasiparticle states induces a characteristic enhancement of $\sigma_1(T)$, the so-called coherence peak, which occurs near below T_c. Quasiparticle scattering affects it in a characteristic manner. The peak is most strongly pronounced in the dirty limit ($l \ll \xi_0$) but disappears in the clean limit ($l \gg \xi_0$). Simultaneously, for $l \ll \xi_0$, $\sigma_2(T)$ exhibits a slightly increased curvature, which decreases for $l \gg \xi_0$. The strength of the phonon-mediated pairing interaction affects $\sigma(T)$ as follows. An increase of the electron-phonon coupling constant λ_{ep} leads to a reduction of the coherence peak, while at the same time the curvature of $\sigma_2(T)$ increases. In conclusion, the differently changing signatures of $\sigma_1(T)$ and $\sigma_2(T)$ provide a simple phenomenological distinction of effects caused by quasiparticle scattering and pair-coupling strength.[26]

In the local limit, the surface impedance is determined by $\sigma(T)$ as

$$Z_S = \frac{i\omega\mu_0}{\sqrt{\sigma}} = R_S + i\omega\mu_0\lambda. \tag{4}$$

In the BCS limit, for $T \leqslant 0.5T_c$, the surface resistance and the change of the penetration depth can be approximated by

$$R_S(T) \propto \frac{(\hbar\omega)^2}{k_B T} \ln\left(\frac{4k_B T}{\omega}\right)\exp(-\Delta/k_b T),$$

$$\Delta\lambda(T) \propto \sqrt{\frac{\pi\Delta}{2k_b T}}\exp(-\Delta/k_B T). \tag{5}$$

The exponential temperature dependence remains valid even for strong electron-phonon coupling, but with a larger value of the reduced energy gap. This so-called scaled BCS approach was proven to describe the surface resistance of strongly coupled superconductors in the framework of Eliashberg theory very well.[27,28]

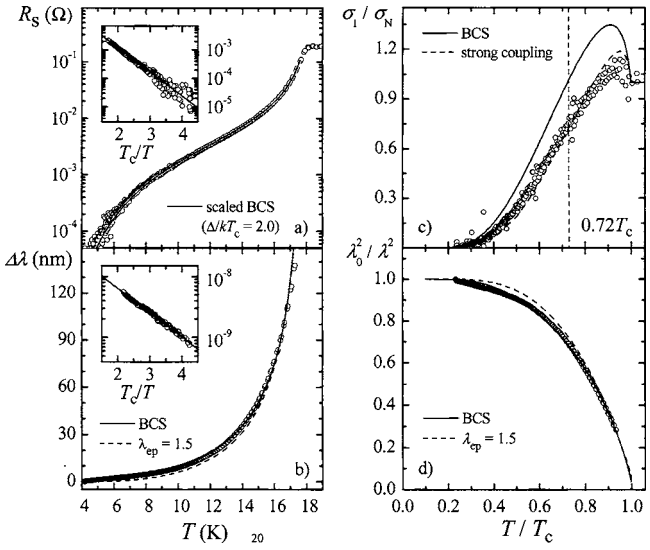

FIG. 2. Typical results for the temperature-dependent surface resistance (a) and penetration depth (b), as measured (circles) and calculated (curves) for undoped Nb_3Sn films at 87 GHz. The insets illustrate the exponential T dependence (further explanation in the text). Real (c) and imaginary (d) parts of the temperature-dependent microwave conductivity, as deduced from the measured surface-impedance data (circles), and as calculated (curves). All data are displayed in normalized units.

IV. EXPERIMENTAL RESULTS

A. Microwave response of undoped Nb_3Sn films

Figure 2 displays typical measured results (symbols) for the surface impedance [R_S and $\Delta\lambda$ in (a) and (b)] and the complex conductivity [σ_1/σ_N and $(\lambda_0/\lambda)^2$ in (c) and (d)] for undoped Nb_3Sn films. The experimental data are compared with the predictions of different theoretical models (curves). To exclude effects due to grain boundary coupling, as documented in Ref. 21, only data for films with an average grain size $d_G \geqslant 700$ nm were selected.

In detail, in Fig. 2(a), the measured $R_S(T)$ is fitted to numerical results calculated within the framework of the scaled BCS theory. The calculations were performed with fixed values for T_c and l [as deduced from the resistivity, $l \propto 1/\rho_N(T_c)$], varying only the parameters Δ/kT_c, λ_L, and ξ_0. An excellent agreement between measured and theoretical data was achieved with the values listed in Table I. The inset in Fig. 2(a) illustrates the exponential dependence of $R_S(T)$ further. The approximation according to Eq. (5) (line) yielded gap values that agreed with the numerically extracted results.

Figure 2(b) displays fits of $\Delta\lambda(T)$ to numerical results based on BCS theory[29] (solid curve) and Eliashberg theory[30] (dashed curve), respectively, for the local limit. For the latter, an electron-phonon coupling $\lambda_{ep}=1.5$ was used, to comply with the experimental Δ/kT_c value of 2.0.[31] The fits were performed by fixing T_c to the measured value of 18 K and varying the parameter λ_0, which is related to the London penetration depth λ_L by $\lambda_0=\lambda_L(1+\pi\xi_0/2l)^{1/2}$ (Ref. 32). We have found that the BCS theory always fitted the measured temperature dependences better, but the resulting values for the London penetration depth were systematically lower by a factor of about 2. In contrast, λ_L values resulting from the strong-coupling theory corresponded to the expected value, while the temperature dependence conspicuously deviated from the measured data. To account for quasiparticle scattering, the fits implied the dirty limit, but the results for λ_0 remained unaffected at a level of less than 5%, even by moving to the clean limit.

As can be seen in the inset in Fig. 2(b), $\Delta\lambda(T)$ can be approximated by an exponential dependence up to $T<T_c/2$, although implying gap values of up to 50% smaller than expected from the $R_s(T)$ data. These deviations reflect that the temperature dependence of the penetration depth was less curved than expected.

Figure 2(c) displays the temperature-dependent quasiparticle conductivity, as deduced from the measured $Z_S(T)$ according to Eq. (4), and as calculated with the BCS theory (solid curve) and the Eliashberg theory (dashed curve).[26] An electronic mean free path of $l=12$ nm has been used throughout. For the case of strong coupling, the electron-phonon coupling spectrum $\alpha^2F(\omega)$ enters the numerical computation. We have taken a spectrum published in the literature[33] for Nb_3Sn samples prepared by a Sn-diffusion process similar to our films. However, evaluating $\alpha^2F(\omega)$ yielded a coupling constant of $\lambda_{ep}=1.08$, which is lower than expected for Nb_3Sn. This discrepancy has to be kept in mind when comparing the numerical and experimental data.

The measured data indeed indicate the signature of strong electron-phonon coupling. The slight deviations of the experimental data from the calculated curve can be attributed to the $\Delta\lambda(T)$ anomaly, which is mapped onto the temperature dependence of $\sigma_1(T)$. Furthermore, the fact that the measured coherence peak is lower than the computed result reflects a higher λ_{ep} value than suggested by Ref. 33.

Finally, in Fig. 2(d), the measured and calculated $\lambda_0^2/\lambda^2(T)$ data are displayed. According to the values for λ_L, ξ_0, and l listed in Table I, a value of $\lambda_0=125$ nm was used for all curves displayed in Fig. 2. The unexpected temperature dependence of the penetration depth becomes most obvious for the scaling used in Fig. 2(d).

B. Surface impedance of Ti-doped Nb_3Sn films

The effects of Ti doping on the temperature dependent surface resistance and the change of the penetration depth are illustrated in Figs. 3(a) and 3(b). Shown are selected data for three films with different doping concentrations, $\chi_{Ti}=0$, 0.13, and 0.25.

Figure 3(a) displays the variation of $R_S(T)$ with χ_{Ti}. The normal-state resistance increases monotonically with an increasing doping level, reflecting the dependence of $\rho_N(T_c)$ on χ_{Ti}. In contrast, a nonmonotonic variation of R_S is observed in the superconducting state, as further illustrated by the inset in Fig. 3(a). The R_S values at $T=0.72T_c$ indicate a slightly increased level for small Ti concentrations ($\chi_{Ti}<0.13$), followed by a minimum around $\chi_{Ti}\approx 0.3$. For $\chi_{Ti}\geqslant 0.6$, R_S exceeded the level of undoped films for all temperatures. Furthermore, a finite residual resistance was observed, which we attribute to the presence of unreacted Ti. The curve repre-

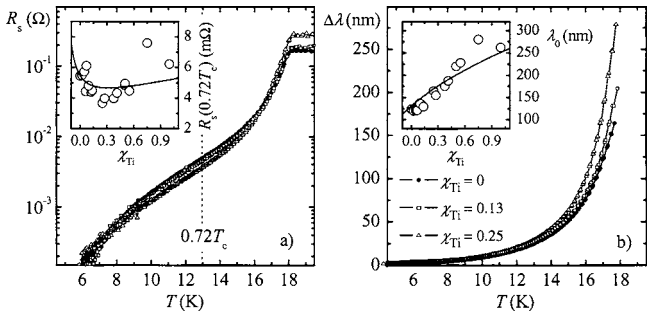

FIG. 3. Temperature-dependent surface resistance (a) and penetration depth (b) for three films with different Ti concentrations. The insets indicate the variations of $R_S(0.72T_c)$ and λ_0 with the doping level in comparison with the theoretical expectations described in the text.

sents the two-fluid model for $R_S \propto \sigma_1 \lambda_0^3$, assuming $\sigma_1 \propto l$ and $\lambda_0 \propto (1+\pi\xi_0/2l)^{1/2}$, as before. In qualitative accordance with the experimental data, the calculated curve displays a minimum near $\chi_{Ti} \approx 0.3$, where the electronic mean free path equals the coherence length ($l=\xi_0$).[32] Quantitatively, this feature is shallower than observed in experiment.

Figure 3(b) depicts the doping dependence of $\Delta\lambda(T)$. To determine λ_0, the measured data were fitted to the temperature dependence calculated for $\lambda_{ep}=1.5$, as discussed above. The inset in Fig. 3(b) shows the resulting λ_0 values (circles), which monotonically increase with increasing χ_{Ti}. The curve indicates the behavior expected for a reduction of the mean free path caused by the quasiparticle scattering.

C. Energy gap, quasiparticle conductivity, and transition temperature

To illustrate the impact of Ti doping on the electron-phonon coupling strength more closely, Fig. 4 summarizes the results for the reduced energy gap (a), the normalized quasiparticle conductivity $\sigma_1/\sigma_N(0.72T_c)$ (b), and the inductively measured transition temperature (c). The reduced energy gap Δ/kT_c was deduced from the exponential $R_S(T)$ dependences according to Eq. (5). The normalized quasiparticle conductivity at a fixed temperature near below the position of the coherence peak can be considered representative of the peak height,[26] as indicated in Fig. 2(c). The error bars in Fig. 4(b) indicate a typical statistical parameter spread. The experimental evaluation of the maximum value of σ_1 would be less accurate than the choice of $\sigma_1/\sigma_N(0.72T_c)$ because of the greater impact of data scatter at the peak.

Figure 4(a) indicates a slight suppression of the reduced energy gap for $\chi_{Ti}<0.13$, with a minimum value of $\Delta/kT_c \approx 1.75$. A further enrichment of Ti inverts this behavior, with Δ/kT_c rising to a maximum value of $\Delta/kT_c \approx 2.70$. A corresponding variation was observed for the quasiparticle conductivity for the two ranges of weak and strong doping [Fig. 4(b)]. For $\chi_{Ti}<0.13$, a slight increase of $\sigma_1/\sigma_N(0.72T_c)$ is indicated compared to undoped films, while for $\chi_{Ti}>0.13$, a reduction of $\sigma_1/\sigma_N(0.72T_c)$ is observed, at least up to about $\chi_{Ti} \geqslant 0.75$.

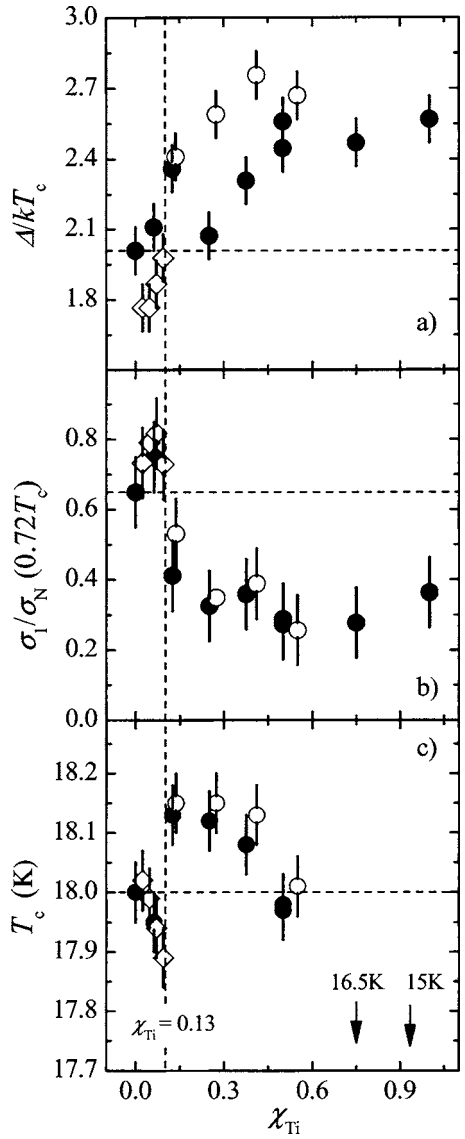

FIG. 4. Comparison of the doping-level dependences of the reduced gap (a), the quasiparticle conductivity at $0.72T_c$ (b), and the inductively measured transition temperature (c). The different symbols represent the differently prepared samples (see Fig. 1). The line at $\chi_{Ti}=0.13$ indicates the crossover from weak to strong doping (further explanations in the text).

According to Fig. 4(c), the overall doping-induced variation of T_c remained small up to $\chi_{Ti}=0.6$. At a closer look, reduced T_c values are noticed for $\chi_{Ti}<0.13$, reaching a minimum of $T_c=17.85$ K, while higher Ti concentrations caused a maximum of T_c at 18.15 K. The two highest-doped samples eventually had distinctly reduced transition temperatures of $T_c=16.5$ K ($\chi_{Ti}=0.75$) and $T_c=15$ K ($\chi_{Ti}=1$), accompanied by a broadening of the transition width from $\Delta T_c=0.1$ K to $\Delta T_c \geqslant 0.3$ K.

D. Temperature-dependent penetration depth

Finally, the effect of Ti doping on the temperature-dependent change of the penetration depth is discussed in greater detail. The graphs shown in Fig. 5 are displayed on

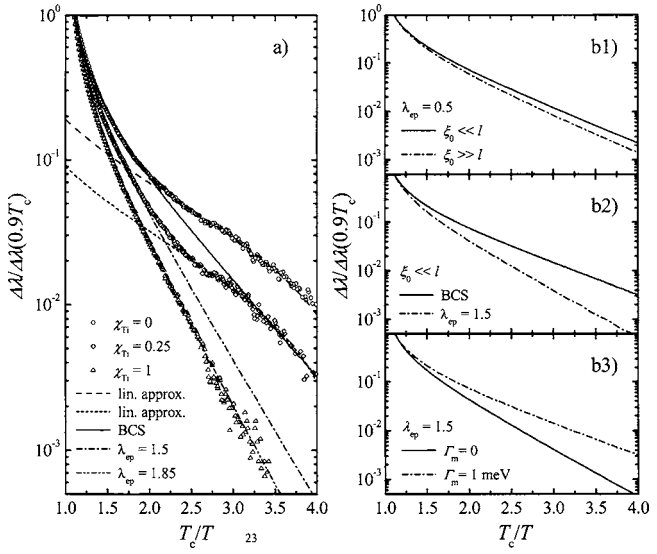

FIG. 5. (a) Comparison of the temperature-dependent variation of the penetration depth measured for different Ti concentrations (symbols) and as calculated (curves). Effects of quasiparticle scattering (b1), electron-phonon coupling (b2), and magnetically induced pair breaking (b3) on $\Delta\lambda(T)$. Γ_m indicates the pair-breaking rate (Ref. 30).

reduced semilogarithmic scales, to highlight the curvature of $\Delta\lambda(T)$. The measured data are compared with the results of numerical calculations.

Figure 5(a) displays typical results measured for three samples with different doping rates [$\chi_{Ti}=0$ (circles, top), 0.25 (diamonds, middle), and 1 (triangles, bottom)] but which are otherwise identical. Obviously, the steepness of $\Delta\lambda(T)$ increases markedly for increasing doping levels χ_{Ti}. Similar effects could be simulated numerically by varying the quasiparticle scattering rate [Fig. 5(b1)], the electron-phonon coupling [Fig. 5(b2)], or the pair breaking due to magnetic impurities [Fig. 5(b3)]. The steepness of the temperature-dependent penetration depth increases for increasing scattering and coupling strength, but decreases for increasing pair breaking. As can be seen in Fig. 5(a), at high temperatures ($1<T_c/T<2$), measured and calculated data are in accordance if the effect of doping is considered to enhance the electron-phonon coupling strength. At low temperatures ($T_c/T>2$) and small Ti concentrations, however, the measured data display a linear temperature dependence (dashed lines), whose contribution to the overall behavior gradually decreases for increasing doping level. This contribution eventually disappears in case of the highest investigated Ti concentrations, where the calculated curve fits the experimental $\Delta\lambda(T)$ data over the whole investigated temperature range. The corresponding electron-phonon coupling constant $\lambda_{ep}=1.85$ is consistent with the large energy gap $\Delta/kT_c=2.6$ deduced from the $R_S(T)$ data.[31]

In total, Ti doping affects $\Delta\lambda(T)$ in two ways, namely, an increasing curvature of the temperature dependence and a reduction of the low-temperature "anomaly."

V. DISCUSSION

An enhanced quasiparticle scattering rate due to the gradually increasing occupation of Nb sites by Ti atoms is the most likely case that, at the same time, yields a consistent theoretical description of the measured data. In turn, its effect on the surface impedance provides a relative measure of the effective doping level. Additional scattering centers can be provoked by the Ti atoms themselves but also by the associated stoichiometry deviations, which are known to strongly increase the resistivity. Phenomenologically, enhanced scattering is reflected by the simultaneously increasing values of the normal-state resistivity $\rho_N(T_c)$ and the penetration depth λ_0. For $\chi_{Ti}<0.13$, the impact of scattering is further apparent from the simultaneously rising height of the coherence peak and the curvature of $\Delta\lambda(T)$. Finally, the slightly reduced values of Δ/kT_c and T_c at low doping, $\chi_{Ti}<0.13$ (Fig. 4), can also be related to an enhanced quasiparticle scattering rate, due to the related broadening and lowering of the $N_N(E)$ peak close to E_F. Thus, a doping-induced quasiparticle scattering is apparent over the whole investigated doping range, and it seems to be even the dominant mechanism for doping levels up to $\chi_{Ti}\cong 0.13$.

Although even the nonmonotonic behavior of $R_S(\chi_{Ti})$ can be qualitatively described by an increasing scattering rate, significant discrepancies between experimental data and theoretical predictions remain. Furthermore, the effects observed for $\chi_{Ti}>0.13$ require additional explanations. Phenomenologically, the increasing value of the reduced energy gap, the decreasing height of the coherence peak, and the increasing curvature of $\Delta\lambda(T)$ are in accordance with the expectations for an enhanced electron-phonon coupling strength. Possible reasons for a strengthening of the pair interaction are, e.g., an altered lattice parameter, an extended phonon spectrum, or an enhanced quasiparticle DOS $N_N(0)$. Changes in the number of occupied quasiparticle states near the peak in the density of states, the peak height, and its proximity to the Fermi level are proven to affect the superconducting properties of Nb_3Sn and, in particular, its electron-phonon coupling strength.[34] Such changes were associated with stoichiometry deviations,[35] but could also be induced by Ti doping. In fact, in Ref. 13, the Ti-doping-induced alteration of the critical temperature was explained on the basis of an electron-phonon coupling strength altered by the electronic DOS. Hence, the T_c values were interpreted to directly reflect the doping-level dependence of λ_{ep}. Even though this explanation seems to be relevant, it cannot describe all of our observations, like the suppression of T_c at higher doping levels. However, it is reasonable to assume that unreacted Ti induces structural disorder effects that are known to strongly suppress T_c in A15 superconductors.[13]

The reason, finally, for the unexpected weakly curved temperature-dependent penetration depth of undoped Nb_3Sn films remains unclear. Potential impact on such behavior could have the granular structure of the samples in terms of the temperature-dependent Josephson penetration depth.[36] As detailed in Ref. 21, our two-step process enables us to adjust the average grain size d_G, as this parameter is controlled by the thickness of the Nb-precursor film. Based on systematic studies, granular effects were indeed shown to modify the superconducting properties of Nb_3Sn films, leading even to a specific dependence of λ_0 on d_G. However, the $\Delta\lambda(T)$ behavior described in the present study did not exhibit any corre-

lation with the grain size of the films. Moreover, the amount of small grains with $d_G < \lambda_0$ within one sample can be considered negligible. Therefore, granularity cannot explain the depicted $\Delta\lambda(T)$ behavior. While further studies are required to answer this question, the variation of the microwave properties of the Nb_3Sn films with the Ti-doping level still yields a consistent picture.

VI. CONCLUSIONS

In conclusion, we reported the synthesis and microwave characterization of Ti-doped high-quality Nb_3Sn films on sapphire. The temperature-dependent microwave response was analyzed at 87 GHz. Surface resistance and the real part of the complex conductivity of undoped samples were in accordance with the expectations for a strong-coupling superconductor, but deviations of the measured $\Delta\lambda(T)$ from theoretical expectations were uncovered, hinting at an approximately linear temperature dependence at $T < 0.5T_c$. Doping the Nb_3Sn films with Ti caused a monotonic increase in the resistivity and the penetration depth. Furthermore, nonmonotonic variations of the reduced energy gap, the quasiparticle conductivity, and the transition temperature were observed. The impact on the temperature dependence of $\Delta\lambda(T)$ was an increased curvature and a suppression of the low-temperature anomaly. The microwave data were evaluated in terms of quasiparticle scattering and electron-phonon coupling strength, both of which were assumed to be related to a doping-dependent modification of the peaked quasiparticle DOS near the Fermi level. Within this framework, most experimental observations could be consistently explained. Our study demonstrates that even classical superconductors like Nb_3Sn continue to provide an interesting area of research of superconductivity.

ACKNOWLEDGMENTS

The authors would like to thank Günter Müller at the University of Wuppertal for valuable discussions and F. Marsiglio at the University of Alberta, Edmonton, for performing the numerical calculations of the quasiparticle conductivity.

[1] J. G. Bednorz and K. A. Müller, Z. Phys. B: Condens. Matter **64**, 189 (1986).
[2] J. Nagamatsu, N. Nakagawa, T. Muranaka, Y. Zenitani, and J. Akimitsu, Nature **410**, 63 (2001).
[3] T. P. Orlando, E. J. McNiff, Jr., S. Foner, and M. R. Beasley, Phys. Rev. B **19**, 4545 (1979).
[4] J. Labbé and J. Friedel, J. Phys. (Paris) **27**, 153 (1966); **27**, 303 (1966).
[5] W. Weber, Physica B & C **126B**, 217 (1984).
[6] T. Müller-Heinzerling, J. Fink, and W. Weber, Phys. Rev. B **32**, 1850 (1985).
[7] J. Bouvier and J. Bok, in *The Gap Symmetry and Fluctuations in High T_c-Superconductors*, edited by J. Bok *et al.* (Plenum Press, New York, 1998).
[8] M. Perpeet, M. A. Hein, G. Müller, H. Piel, and J. Pouryamout, J. Appl. Phys. **82**, 5021 (1997).
[9] C. T. Wu, R. T. Kampwirth, and J. W. Hafstrom, J. Vac. Sci. Technol. **14**, 134 (1977); R. T. Kampwirth, J. W. Hafstrom, and C. T. Wu, IEEE Trans. Magn. **MAG-13**, 315 (1977); A. Andreone, A. Cassinese, A. Di Chiara, M. Ivarone, F. Palomba, A. Ruosi, and R. Vaglio, J. Appl. Phys. **82**, 1736 (1997); IEEE Trans. Appl. Supercond. **7**, 1772 (1997).
[10] L. H. Allen, M. R. Beasley, R. H. Hamond, and J. P. Turneaure, IEEE Trans. Magn. **MAG-23**, 1405 (1987).
[11] W. N. Hardy, D. A. Bonn, D. C. Morgan, R. Liang, and K. Zhang, Phys. Rev. Lett. **70**, 3999 (1993).
[12] F. Giubileo, D. Roditchev, W. Sacks, R. Lamy, D. X. Thanh, J. Klein, S. Miraglia, D. Fruchart, J. Marcus, and P. Monod, Phys. Rev. Lett. **87**, 177008 (2001).
[13] M. Suenaga, D. O. Welch, R. L. Sabatini, O. F. Kamerer, and S. Okuda, J. Appl. Phys. **59**, 840 (1986).
[14] H. Piel, Proceedings of the Workshop on RF Superconductivity, Karlsruhe, 1980, KFK-report No. 3019, edited by M. Kuntze, p. 85; A. M. Portis, *Electrodynamics of High-Temperature Superconductors*, Lecture Notes in Physics 48 (World Scientific, Singapore, 1993); M. A. Hein, *Physics and Applications of High-Temperature Superconductor Thin Films and Devices*, Vol. 155 (Springer, Heidelberg, 1999).
[15] S. B. Nam, Phys. Rev. **156**, 470 (1967); **156**, 487 (1967).
[16] M. Perpeet, Ph.D. thesis, University of Wuppertal, 1999.
[17] M. Perpeet, A. Cassinese, M. A. Hein, T. Kaiser, G. Müller, and H. Piel, IEEE Trans. Appl. Supercond. **9**, 2496 (1999).
[18] M. Perpeet, W. Diete, M. A. Hein, S. Hensen, T. Kaiser, G. Müller, and H. Piel, Appl. Supercond. **158**, 101 (1997).
[19] J. Halbritter, J. Supercond. **5**, 171 (1992).
[20] L. Rinderer, L. Saur, and J. Wurm, Z. Phys. **174**, 405 (1963); P. Kneisel, H. Küpfer, W. Schwarz, O. Stolz, and J. Halbritter, IEEE Trans. Magn. **MAG-13**, 496 (1977); G. Arnolds, H. Heinrichs, R. Mayer, N. Minatti, H. Piel, and W. Weingarten, IEEE Trans. Nucl. Sci. **NS-26**, 3775 (1979); G. Müller, P. Kneisel, D. Mansen, H. Piel, J. Pouryamout, and R. W. Röth, in *Proceedings of the 5th European Particle Accelerator Conference*, Sitges, Barcelona, 1995, edited by S. Myers *et al.* (IOP Publishing, Bristol/Philadelphia, 1996), Vol. 3, p. 2085.
[21] M. A. Hein, M. Perpeet, and G. Müller, IEEE Trans. Appl. Supercond. **11**, 3434 (2001).
[22] N. Klein, G. Müller, H. Piel, B. Roas, L. Schultz, U. Klein, and M. Peiniger, Appl. Phys. Lett. **54**, 757 (1989); S. Hensen, G. Müller, C. T. Rieck, and K. Scharnberg, Phys. Rev. B **56**, 6237 (1997).
[23] M. Tinkham, *Introduction to Superconductivity* (McGraw-Hill, New York, 1975).
[24] J. R. Waldram, *Superconductivity of Metals and Cuprates* (Institute of Physics Publishing, Bristol, 1996).
[25] W. N. Hardy, S. Kamal, and D. A. Bonn in *The Gap Symmetry and Fluctuations in High T_c-Superconductors*, edited by J. Bok *et al.* (Plenum Press, New York, 1998).
[26] F. Marsiglio, Phys. Rev. B **44**, 5373 (1991); F. Marsiglio, J. P.

Carbotte, R. Akis, D. Achkir, and M. Poirier, *ibid.* **50**, 7203 (1994).
[27] R. Blaschke and R. Blocksdorf, Z. Phys. B: Condens. Matter **49**, 99 (1982).
[28] R. Blaschke, A. Phillipp, and J. Halbritter, *Proceedings of the 4th Conference on Superconductivity in d- and f-Band Metals*, Karlsruhe, 1982, (unpublished), and related references.
[29] B. Mühlschlegel, Z. Phys. **155**, 313 (1959).
[30] S. D. Adrian, M. E. Reeves, S. A. Wolf, and V. Z. Kresin, Phys. Rev. B **51**, 6800 (1995).
[31] D. A. Rudman and M. R. Beasley, Phys. Rev. B **30**, 2590 (1984).
[32] J. Halbritter, Z. Phys. **266**, 209 (1974).
[33] L. Y. L. Shen, Phys. Rev. Lett. **29**, 1082 (1972).
[34] J. Labbe, S. Barisic, and J. Friedel, Phys. Rev. Lett. **19**, 1039 (1967).
[35] D. F. Moore, R. B. Zubeck, J. M. Rowell, and M. R. Beasley, Phys. Rev. B **20**, 2721 (1979); D. A. Rudman, F. Hellman, R. H. Hammond, and M. R. Beasley, J. Appl. Phys. **55**, 3544 (1984); D. A. Rudman and M. R. Beasley, Phys. Rev. B **30**, 2590 (1984).
[36] T. L. Hylton and M. R. Beasley, Phys. Rev. B **39**, 9042 (1989).